

New nitric oxide (NO) nightglow measurements with SPICAM/MEx as a tracer of Mars upper atmosphere circulation and comparison with LMD-MGCM model prediction: Evidence for asymmetric hemispheres

Marie-Ève Gagné,^{1,2} Jean-Loup Bertaux,³ Francisco González-Galindo,⁴
Stella M. L. Melo,^{1,2} Franck Montmessin,³ and Kimberly Strong²

Received 19 March 2013; revised 22 July 2013; accepted 28 September 2013; published 15 October 2013.

[1] We report observations of NO nightglow with the Spectroscopy for the Investigation of the Characteristics of the Atmosphere of Mars (SPICAM) experiment on board the Mars Express (MEx) spacecraft. NO molecules emit an ultraviolet photon when N and O atoms (produced at high altitude in the thermosphere) recombine. Therefore, this emission is a tracer of the atmospheric dynamics in the lower thermosphere where O and N atoms are produced, and below, in the altitude region 50–100 km where the emission is detected. A new retrieval method has been developed to analyze the measurements from this instrument in the stellar occultation mode without slit and retrieve the absolute brightness of the emission. We present the results from the processing of more than 2000 orbits, providing the first global latitude-season distribution of the emission, established over three Martian years. The results are globally consistent with previously available measurements of dedicated limb nightglow obtained during the first Martian year of MEx (MY27). We compared the ensemble of both data sets with the predictions of the Laboratoire de Météorologie Dynamique Mars General Circulation Model (LMD-MGCM), with the addition of the full chemistry of N atoms. We find an overall agreement between the observed and modeled airglow intensities, but discrepancies are also found. The frequency and magnitude of the NO airglow observations show important asymmetries between the Northern and the Southern Hemispheres. There is no detection of emission near the poles during equinox conditions, while the model predicts that it should be most intense because of a circulation with two descending branches at the poles.

Citation: Gagné, M.-È., J.-L. Bertaux, F. González-Galindo, S. M. L. Melo, F. Montmessin, and K. Strong (2013), New nitric oxide (NO) nightglow measurements with SPICAM/MEx as a tracer of Mars upper atmosphere circulation and comparison with LMD-MGCM model prediction: Evidence for asymmetric hemispheres, *J. Geophys. Res. Planets*, 118, 2172–2179, doi:10.1002/jgre.20165.

1. Introduction

[2] The atmospheres of Venus and Mars have a similar composition ($\sim 95\%$ CO₂ and 3–4% N₂), and therefore, we may expect some other similarities. In the thermospheres of both planets, CO₂ and N₂ molecules are photodissociated

by solar ultraviolet (UV) and extreme ultraviolet radiation. O and N atoms are transported by the general circulation from the dayside to the nightside, where they recombine in O₂ and NO molecules, as recognized by their nightglow emission at 1.27 μm and in the UV, respectively. These emissions are a direct tracer of the atmospheric dynamics, and their study therefore provides a powerful diagnostic of the general circulation in the upper atmosphere.

[3] While these emissions were already identified in Venus several decades ago (*Connes et al.* [1979] for O₂ and *Feldman et al.* [1979] and *Stewart et al.* [1979] for NO), it was not until the Mars Express (MEx) electrostatic analyzer mission, in orbit since 2003 around the planet Mars, that they were observed. The UV emission from the NO δ and γ bands was discovered as a nightglow by the SPICAM UV channel (SPICAM is the acronym for Spectroscopy for the Investigation of the Characteristics of the Atmosphere of Mars) and first reported in 2005 [*Bertaux et al.*, 2005], while the O₂ emission from oxygen atom recombination was

¹Space Science and Technology, Canadian Space Agency, Saint-Hubert, Québec, Canada.

²Department of Physics, University of Toronto, Toronto, Ontario, Canada.

³LATMOS, Université de Versailles Saint-Quentin/CNRS, Guyancourt, France.

⁴Instituto de Astrofísica de Andalucía, CSIC, Glorieta de la Astronomía, Granada, Spain.

Corresponding author: M.-È. Gagné, Canadian Centre for Climate Modelling and Analysis, University of Victoria, Victoria, BC, Canada. (Marie-Eve.Gagne@ec.gc.ca)

discovered by the Observatoire pour la Minéralogie, l'Eau, les Glaces et l'Activité, also on Mars Express [Bertaux *et al.*, 2012], and also observed by the Compact Reconnaissance Imaging Spectrometer for Mars (CRISM) on the Mars Reconnaissance Orbiter [Clancy *et al.*, 2012].

[4] After the 2005 NO discovery, Cox *et al.* [2008] analyzed 21 orbits of SPICAM containing limb observations of these NO UV emissions: The maximum brightness of the observations is in the range 0.2 to 10.5 kR, with a mean value of 1.2 ± 1.5 kR, and it peaks between 55 and 92 km in altitude, with a mean value of 73.0 ± 8.2 km. Cox *et al.* [2008] concluded from their analysis that the higher the latitude of the measurements, the lower is the altitude of the peak, which they linked to the behavior of constant pressure surfaces that are higher close to the equator. Also, they found that the highest brightness values are near 60°S , but they could not infer a real systematic dependence between the peak altitude and the peak brightness. The spatial distribution of the NO nightglow as a function of the local time supports the hypothesis of a global transport mechanism generating a downward flux of N and O atoms on the night-side that recombine to produce the NO emissions [Bertaux *et al.*, 2005].

[5] A description of the characteristics of the SPICAM instrument can be found in the work of Bertaux *et al.* [2006]. The UV spectrometer can be used in several modes. For limb dayglow or nightglow measurements, a slit is placed at the focus of the single parabolic off-axis mirror, providing a spectral resolution of ~ 1.5 or ~ 6 nm, depending on which part of the slit is selected when reading out the charge-coupled device (CCD, coupled to an image intensifier). When used for a stellar occultation sounding of the atmosphere, the slit is taken out to account for some possible mispointing of the spacecraft which would affect the detection of the faint signal. However, in this case, diffuse emission at the limb is an extended source, which adds to the star signal as a stray light. For a given intensity in kR, the recorded signal is much larger when the slit is not in place, given the spatial extent of the emission at the limb.

[6] As a matter of fact, in the case of Venus and SPICAV (Spectroscopy for the Investigation of the Characteristics of the Atmosphere of Venus) operations from Venus Express (VEx), the NO emission is in many cases so intense that it saturates the occultation measurements and the SPICAV/VEx team is now using the widest section of the slit to perform stellar occultations. But the NO “stray light” recorded during a normal star occultation (no slit) can be extracted and analyzed to estimate the emission brightness. This was done for SPICAV at Venus [Royer *et al.*, 2010], adding a large number of NO observations to those obtained using the slit for monitoring nightglow.

[7] We have taken the approach of Royer *et al.* [2010] and scrutinized 2215 stellar occultations performed by SPICAM to look for the stray light emission at the limb of Mars. We extracted NO signal from 128 of the 2215 occultations, allowing a much better global view than that from the rather sparse dedicated nightglow limb data (29 independent positive detections over 2 years 2004–2006 [Cox *et al.*, 2008]). The present data set extends from $L_s = 44^\circ$ for Martian year (MY) 27 to $L_s = 326^\circ$ in MY 29, spanning almost three Martian years in total. In addition, we have developed an inversion technique (spatial/spectral deconvolution), which

allows the retrieval of 2-D snapshot of the airglow layer brightness distribution within one occultation, projected at the limb (altitude and horizontal distance, because the spacecraft is also moving horizontally during one occultation). This is possible because each recorded spectrum is the convolution of the spatial distribution of emission at the limb along the field of view (FOV) covered by one measurement band, by the actual spectrum of the emission. Here we proceed to the direct deconvolution of the observed signal to retrieve the brightness distribution along the FOV, while in the method of Royer *et al.* [2010] used for Venus, the observed signal was fitted manually by a forward model, assuming a Chapman layer for the vertical distribution of the NO airglow. With this new method, there is no need for any prior assumption about the vertical structure of the emission. The technique is described in Gagné [2013]. The results are then compared with the analysis of the SPICAM limb observations of the NO emission by Cox *et al.* [2008], which is the only published data set for this Mars atmospheric emission and which covered only a limited L_s sampling. The observations of the emission are further compared with model simulations of NO airglow to verify our understanding of the photochemical mechanism producing this feature in the Mars atmosphere.

2. Measurements From SPICAM in the Stellar Occultation Mode Without Slit

[8] In the stellar occultation mode, the optical axis of SPICAM is oriented to the direction of a star. While scanning the limb during the spacecraft’s orbital motion, the star slowly disappears behind the planet. The atmospheric spectral transmission is measured by ratioing the signal of the star seen through the atmosphere to the signal of the star recorded outside of the atmosphere a few seconds before the actual occultation. This technique, as well as its advantages and drawbacks, is fully described in the paper of Quémerais *et al.* [2006] and in Bertaux *et al.* [2006]. When there is some limb emission in addition to the star’s signal, the star gives a reference altitude that also allows an altitude to be assigned to the emission, assuming that the emission is in the plane of the limb. It should be noted, however, that it is a minimum altitude, since the emission (which may not be horizontally homogeneous) could be in the foreground, or in the background, and may be projected on the limb at an altitude lower than its actual altitude. Royer *et al.* [2010] explain in details the possible geometries of the NO airglow layer and the difficulty that the problem of nonspherical geometry adds to the accuracy of a retrieval. This feature of our geometry should always be kept in mind in the following.

[9] The NO emission may be disentangled from the star light because SPICAM has five simultaneous measurement field of views (FOVs), in five contiguous bands, each covering $0.09^\circ \times 2^\circ$ or $0.18^\circ \times 2^\circ$. The central band collects the flux of the star, while the outer bands collect the limb emission on each side of the star. The use of numerous stellar occultations in this work and the extraction of useful information from $\sim 6\%$ of them allowed us to build the first climatology of NO emission in the Martian atmosphere, which can be used to evaluate the behavior of global circulation models, e.g., their composition and dynamics.

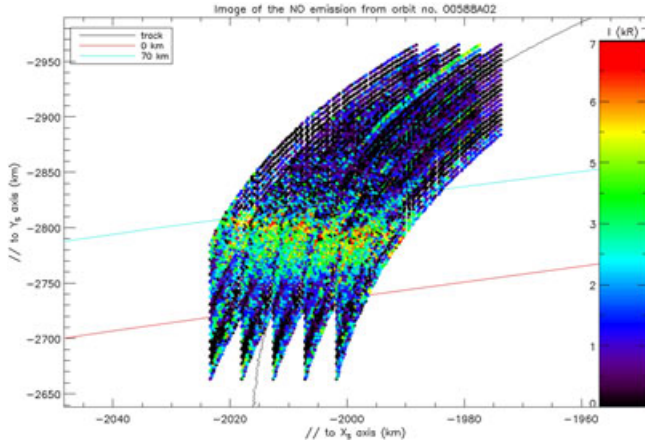


Figure 1. Intensity of the NO emission (color bar) for several spectra as recorded with the five bands of the SPICAM detector. The intensity is plotted as a function of its position with respect to the planet, where the origin of this coordinate system is the center of Mars and the horizontal and vertical axes are parallel ($//$) to the \vec{X}_s and \vec{Y}_s axes of the spacecraft. The brightness from the NO airglow is displayed at the limb, scanned instrument FOV during its occultation sequence, with distances in kilometers with respect to the center of Mars (black line). The brightness is color coded, with red corresponding to the brightest regions; each color dot represents the average brightness of 20 pixels on one line of the detector (along the \vec{Y}_s axis) on one of the five bands (along the \vec{X}_s axis) of the SPICAM detector for one occultation (along track). The emission is seen between the surface of the planet (red line) and 70 km in altitude above the planet's surface (blue line).

3. Observations

[10] Stellar occultation sequences from orbits 485 to 7237, which correspond to nearly three Martian years of observations, or six Earth years, have been examined. Of the 2215 occultations processed, 128 ($\sim 6\%$) produced a detectable NO emission (>0.5 kR). In the remaining sequences, the NO emission was lower than our detection limit in 1992 cases, and in 95 cases, the result was uncertain because of light contamination and therefore discarded from the present study. For each of the 128 occultations that returned a positive NO detection, we proceeded with the inversion technique described in Gagné [2013]. The resulting data set extends the latitudinal and seasonal coverage beyond that of the data used in the Cox *et al.* [2008] study. As an example, the result of this inversion for orbit #0588A01 is shown in Figure 1. During this sequence, an NO airglow layer was observed slightly below 70 km. We also observe on that figure a strong left-to-right altitude trend, with the emission reaching as low as 30 km. As mentioned above, a 2-D snapshot of that sort may be from a nonspherical layer of NO airglow such that the image would contain signal from airglow at the foreground or the background of the tangential altitude and the airglow layer would then appear at an apparent lower altitude.

[11] Figure 2a shows the peak brightness as a function of latitude and season for all successful NO airglow detections, as extracted from the inversion algorithm (color dots). There are more detections of NO emission during the first Martian year, MY27, than later, an interesting interannual variability. Moreover, MY29 contains more occultation sequences than for MY27 but still shows less detection, while the brightness values are higher. A possible explanation of this interannual variability is the solar flux variability from MY27 to MY29.

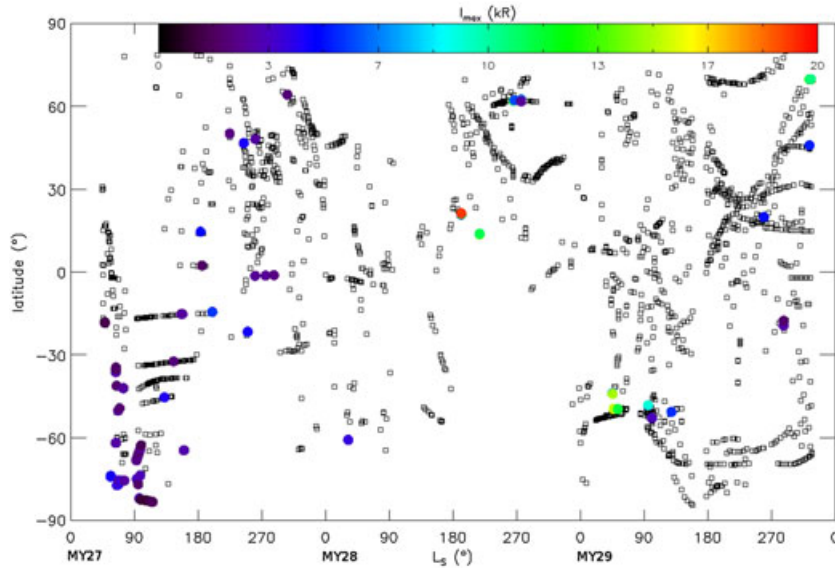


Figure 2. Latitude versus areocentric longitude distribution of the peak brightness from the NO emission as measured by SPICAM. The brightness of the NO emission is represented by color-coded circles (refer to color bar in kR) with red corresponding to the brightest values. Also displayed on the figure are the locations of the 2087 sequences that do not contain a detectable airglow signal (empty squares).

For MY27, the solar activity was still in the declining phase of solar cycle 23, while MY28 and MY29 span the deep minimum of solar activity between solar cycle 23 and solar cycle 24. The mean brightness of the NO airglow in this data set is $4.0 \pm 3.5(1\sigma)$ kR, which is higher than the mean brightness of 1.2 ± 1.5 kR from the work of *Cox et al.* [2008], possibly due to the larger size of our data set. The observations of *Cox et al.* [2008] were taken between MY27 $L_s=72.5^\circ$ and MY28 $L_s=52.5^\circ$. We can see from Figure 2a that the brightest emissions in our data set are found for observations after $L_s=180^\circ$ of MY28. This temporal variability would cause the mean brightness of our data set to be higher than that of *Cox et al.* [2008].

[12] Figure 3 shows the altitudes of the peak emission as a function of latitude; we observe that low-peak altitudes (below 70 km) are observed in the Southern Hemisphere polar region (beyond -60°) in contrast to that in the Northern Hemisphere polar region. No obvious correlation between the peak altitudes and peak brightness is observed from this data set, as is the conclusion from the work of *Cox et al.* [2008]. The mean altitude of the peak from our data set is $83 \pm 24(1\sigma)$ km in agreement with the calculated mean of *Cox et al.* [2008], which is 73.0 ± 8.2 km. The difference in the mean values could again be attributed to the smaller time coverage of the latter observations record.

[13] As is common practice when analyzing the distribution of an airglow feature, we plotted the peak altitude versus the peak brightness of the observations containing a signal from NO airglow (not shown). There seems to be no correlation between these two parameters, and the spread of the values is large as in *Cox et al.* [2008]. This apparent lack of correlation is compatible with the short lifetime of the excited species, i.e., 3.2×10^{-8} s [*Sun and Dalgarno*, 1996] and we expect the NO airglow to be localized and strongly linked to the downward transport of N and O atoms. This vertical transport is subject to dynamical variations, as originally proposed by *Bertaux et al.* [2005]. Such dependency induces significant variability in the altitude of the recombination and hence of the brightness. The dispersion of the peak altitude is larger than in the study of *Cox et al.* [2008]; this is likely due to some noise in our matrix-based inversion

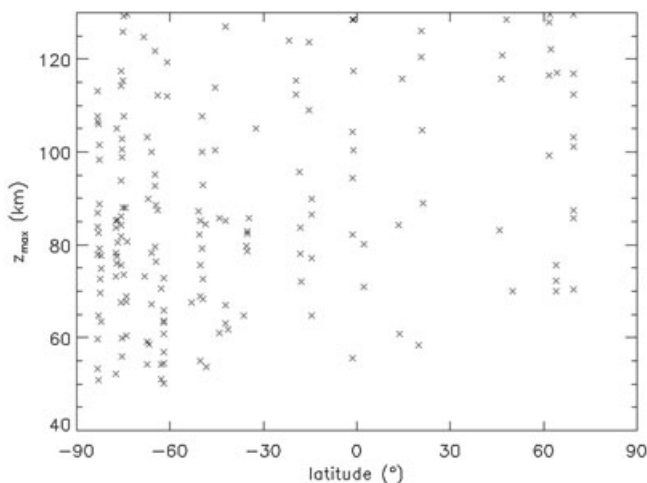


Figure 3. Altitude of the peak NO emission as a function of latitude.

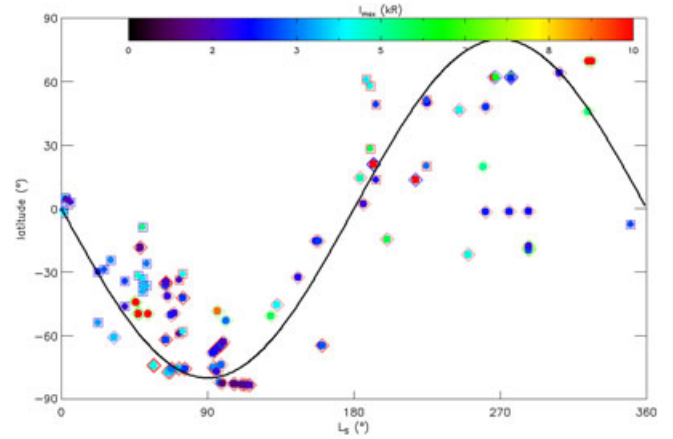


Figure 4. NO observations plotted as a function of L_s and latitude. Color dots overlaid with diamonds represent time and location of the positive detections during that interval, with the color coding the measured limb intensity. Color dots overlaid with squares represent the time, location, and intensity of dedicated limb intensities extracted from *Cox et al.* [2008]. The diamonds and squares in red represent observations for MY27, in blue for MY28, and in green for MY29. The black solid line is a sine curve, $\text{latitude} = -80 \cdot \sin(L_s)$, along which fall (more or less) the positive NO detections of both data sets, this one and that of *Cox et al.* [2008].

process. Indeed, while in the study of *Cox et al.* [2008], all the measurements of one limb crossing are fitted by a layered model, which peak altitude is determined, in our analysis the peak altitude is assigned to the altitude of the brightest point.

[14] On Figure 4, we have plotted all the peak horizontal (limb) intensities from the stellar occultations as a function of latitude and season (solar longitude L_s), folding in the three Martian years of data. There is a clear seasonal pattern of colored circles, which is confirmed by the earlier SPICAM NO data from *Cox et al.* [2008] enclosed within a square. The brightest NO emission is found around a sine curve which may be described as $\text{latitude} = -80 \sin(L_s)$ [*Bertaux et al.*, 2013], with, however, some serious departures from the sine curve in the second part of the Martian year ($L_s=180-360^\circ$).

4. The Model Prediction of NO Emission and Comparison to Observations

[15] The results shown below are the outputs of a one Martian year simulation with the Laboratoire de Météorologie Dynamique Mars General Circulation Model (LMD-MGCM). The model is basically that described in *González-Galindo et al.* [2009] but with an extended photochemical module including nitrogen and ionospheric chemistry from *González-Galindo et al.* [2011] and an improved treatment of the nonlocal thermodynamic equilibrium $15 \mu\text{m}$ cooling that provides realistic temperatures in the mesopause region [*Lopez-Valverde et al.*, 2011]. In total, 93 chemical reactions for the neutral upper atmosphere and the ionosphere are taken into account. This photochemical model is run for layers above 1 Pa (~ 50 km). Below this altitude,

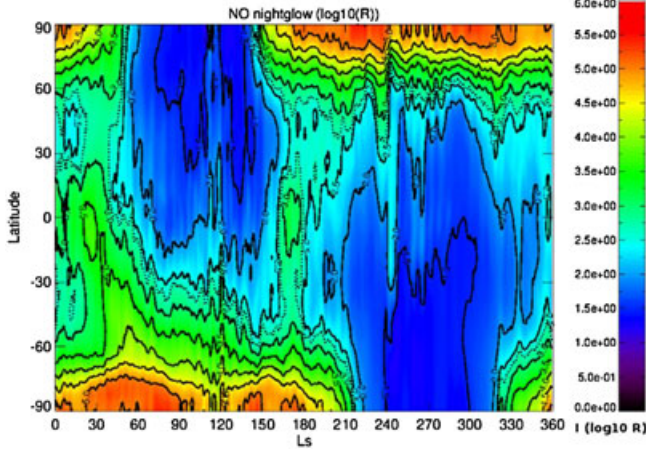


Figure 5. Zonal mean NO nightglow limb integrated intensity (R) predicted by the LMD-MGCM as a function of latitude and L_s at $LT=21$. Note that the color scale is logarithmic: $3=10^3 R$. The dashed contour at the 2.7 level outlines the detection limit of SPICAM.

another photochemical model that does not include nitrogen species but provides a better description of the complex photochemical cycles in the lower atmosphere [Lefèvre *et al.*, 2004] is used. More details about the results from this hybrid photochemical-LMD model with extended NO chemistry can be found in F. Gonzalez-Galindo (3D Martian ionosphere model: I. The photochemical ionosphere

below 180 km, submitted to *Journal of Geophysical Research Planets*, 2013).

[16] Every N and O atoms recombination produces a photon in the NO emission system. The recombination of O+N produces a NO^* molecule in an excited state with a very short radiative lifetime. Therefore, there is no de-excitation by collisions with CO_2 molecules (quenching). The UV photon emission is instantaneous, and the volume emission rate (VER or emissivity) is equal to the rate of NO recombination:

$$\epsilon(NO^*) = \frac{[NO^*]}{\tau} \quad (1)$$

where τ is the lifetime by radiative relaxation of excited NO species and NO^* and $[NO^*]$ is the number density of NO^* :

$$[NO^*] = \frac{k[N][O]}{1/\tau} \quad (2)$$

The rate coefficient k for the recombination reaction of O and N atoms is $2.8 \times 10^{-17} \cdot (300/T)^{1/2} \text{ cm}^3 \text{ s}^{-1}$ [Du and Dalgarno, 1990], where T is the temperature and the radiative lifetime, τ , is taken to be $3.2 \times 10^{-8} \text{ s}$ [Sun and Dalgarno, 1996].

[17] The dust distribution in the lower atmosphere has been shown to have an important influence on the dynamics of the upper thermosphere [Bell *et al.*, 2007]. For the simulation used in this study, we use a climatology of the dust as observed by the Thermal Emission Spectrometer on board the Mars Global Surveyor mission between 1999 and 2001, i.e., MY24–25. A solar flux appropriate for solar average conditions is used. The model is run with its usual vertical

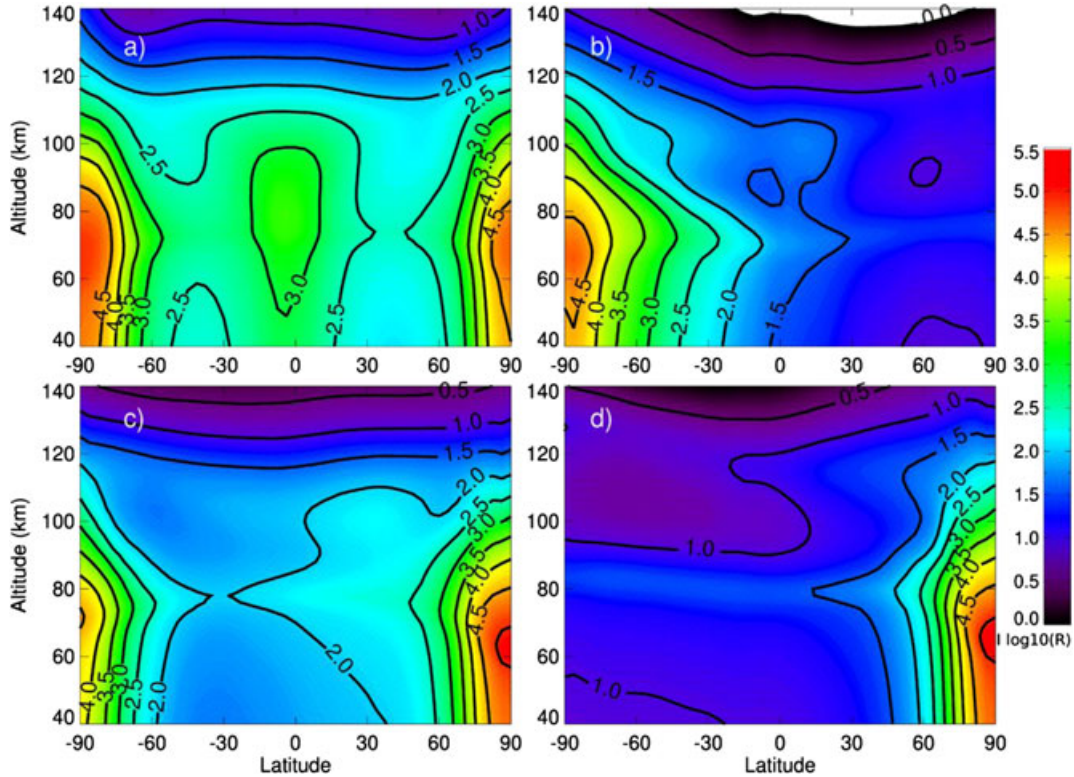


Figure 6. Cross section of zonal mean NO nightglow intensity (R) predicted by the LMD-MGCM for $LT=21$ for different seasons: (a) $L_s=0^\circ-30^\circ$, (b) $L_s=90^\circ-120^\circ$, (c) $L_s=180^\circ-210^\circ$, and (d) $L_s=270^\circ-300^\circ$. Note that the color scale is logarithmic: $3=10^3 R$.

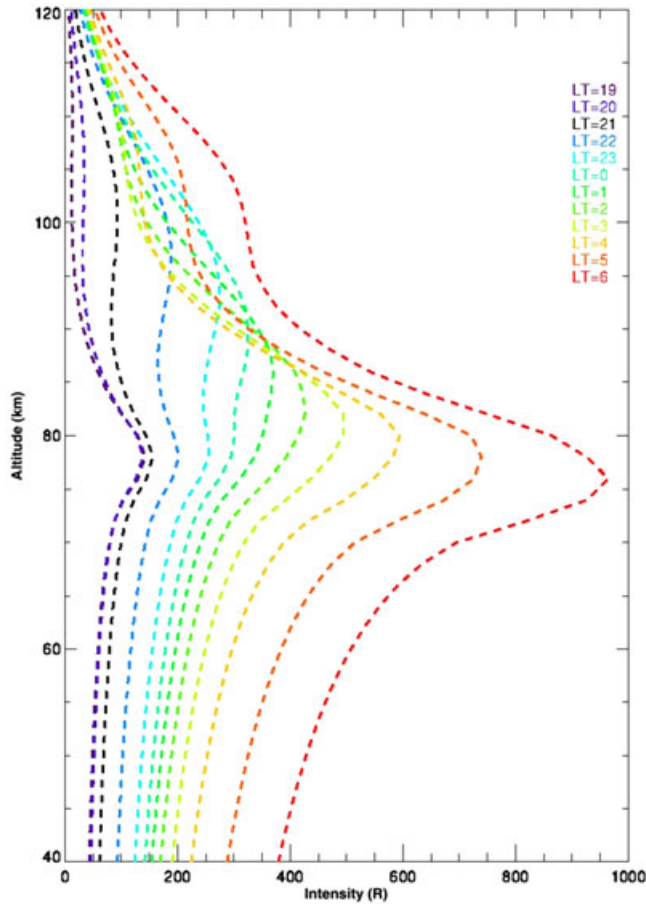


Figure 7. Vertical profiles of the zonal mean NO nightglow emission predicted by the LMD-MGCM for the equator, $\text{lat}=0^\circ$, and $L_s=180\text{--}210^\circ$ at different local times during the night, representative of the daily variability.

(50 layers, from the surface to about 250 km) and horizontal (64×48 grid points) resolution.

[18] Figure 5 shows the zonal mean NO intensity predicted by the model for constant local time $\text{LT}=21$. The maximum intensity is found around the polar regions: During the equinoxes, significant emission is predicted close to both poles, while during solstices, the intensity is concentrated in the winter poles. The maximum emission is in all cases of the order of 100 s of kR, decreasing quickly when going to lower latitudes.

[19] Cross sections of zonal mean intensity predicted by the model for constant local time $\text{LT}=21$ at four different seasons $L_s=0^\circ\text{--}30^\circ$, $L_s=90^\circ\text{--}120^\circ$, $L_s=180^\circ\text{--}210^\circ$, and $L_s=270^\circ\text{--}300^\circ$ are displayed in Figure 5. In the polar regions, the altitude of the peak emission varies between about 60 and 80 km. There is no clear seasonal evolution of the altitude of the peak emission. For most seasons, the altitude of the peak emission tends to be lower in the high-latitude regions, in agreement with *Cox et al.* [2008] observations.

4.1. Comparison for Solstice Conditions

[20] From the observations plotted in Figure 2b, we see that during the southern winter solstice (around $L_s=90^\circ$), all positive detections are between $L_s=60^\circ$ and $L_s=120^\circ$

at latitudes southward of -30° . This is in agreement with the model prediction of Figure 5 that shows NO emissions above 1 kR for $L_s=60^\circ\text{--}120^\circ$ to be found at $\text{lat} > -30^\circ$. The SPICAM detection limit in the present study is about 0.5 kR. However, for latitudes beyond -60° , the model predicts NO intensities above 10 kR and reaching more than 100 kR southward of 75° ; the observations of NO intensities are then much weaker than the model results at high latitudes. We note that SPICAM made stellar occultations around the southern winter solstice at high latitudes for MY27 only (see Figure 2a). For the opposite solstice ($L_s=240^\circ\text{--}300^\circ$), the agreement is less obvious: The detections are spread over a large latitude range, from -20 to $\pm 70^\circ$, while the model predicts a much weaker emission near the equator and emissions of >1 kR to be located northward of $+60^\circ$. Hence, in the Northern Hemisphere, the observed NO emission region extends further toward the equator than the model predicts.

[21] Therefore, the NO data indicate an asymmetric situation between the northern and southern winter solstices, with the observed emissions more extended to lower latitudes for the northern winter solstice, contrary to the prediction of the model. Another observed asymmetry (Figure 5) is that for L_s around 90° ; almost all observations at latitude poleward of -70° contain some NO emission, while around $L_s=270^\circ$, there are plenty of stellar occultations in the high northern latitudes without a detectable signal from NO. The present analysis is somewhat biased by the more numerous positive detections recorded during year MY27, which might have been dynamically special. We note, however, that there are still four detections of NO emission at low latitudes (between -30 and $+30^\circ$) during MY28 and MY29.

4.2. Comparison for Equinox Conditions

[22] The main discrepancy between the model and the observations is rather for equinox conditions, where the model predicts two maxima of emissivity located at both poles, while in the data, we did not detect high emissions at high latitudes, i.e., poleward of latitudes 60° , either around $L_s=0^\circ$ or $L_s=180^\circ$. For $L_s=330^\circ\text{--}30^\circ$, there are no detection of NO emissions in either hemispheres, but SPICAM made only eight stellar occultations sequences for $\text{lat} > 60^\circ$ in both hemispheres, a region where the model predicts emissions detectable by this instrument. For the $L_s=180^\circ$ season, there were many stellar occultations at high latitudes (both in the Southern and Northern Hemispheres), and only three of them showed a detection between $L_s=150^\circ\text{--}210^\circ$ (see Figure 4).

[23] For $L_s=30^\circ\text{--}60^\circ$, the positive detections are at midlatitudes. The model does predict an extended zone of dimmer but detectable (<1 kR but >0.5 kR) emission at middle and low latitudes for this season, as shown on Figure 5. However, at the other equinox ($L_s=180^\circ$), the emission predicted by the model at midlatitudes is less than 1 kR, while the observations show intensities of up to several kR. It has to be taken into account that the model results we are showing here are geographical (zonal mean) and temporal (during 30° of L_s) averages at a single local time ($\text{LT}=21$). The spatial and temporal variability can produce local enhancements of detectable emission, even if the average level predicted by the model is below 1 kR. For example, we show in Figure 7 the zonal mean NO emission profile predicted by the model for the $L_s=180^\circ\text{--}210^\circ$

emission at LT=21 for the equator (black dashed line), together with the profiles obtained for the same season and the same latitude but at different longitudes and different local times (during nighttime, LT between 17 and 9). Significant variability is predicted, so that even if the average peak emission is about 0.1 kR, some of the individual profiles show emissions higher than 1 kR (and thus theoretically detectable by SPICAM). Also, the day-to-day variability and the small-scale variability due to gravity wave propagation can produce further perturbations [Spiga *et al.*, 2012]. It should also be remembered that a constant solar flux is used in the simulation, while the observations encompass three Martian years.

4.3. Comparison of Peak NO Emission Altitude

[24] The distribution of the peak altitude demonstrates a strong variability, with values ranging from 40 to 130 km (Figure 3). However, there seems to be a trend, in which the lowest altitude is increasing from South Pole to North Pole (except for one outlier point). The model shows a peak altitude that is at its lowest in the polar regions (in particular at the winter pole during solstices) and increases toward the lower latitudes (Figure 6). The modeled variability of the peak altitude with latitude (between 60 and 80 km) is not as large as the observed variability. Again, it should be remembered that the model results are spatial and temporal averages.

5. Conclusions

[25] A new data set of NO airglow obtained from the first three Martian years of SPICAM stellar occultations is globally consistent with previously available measurements [Cox *et al.*, 2008]. In general, we find consistency between the results from the processing of the SPICAM stellar occultations presented in this work and the analysis of the SPICAM limb observations by Cox *et al.* [2008]: There is coherence between the time and location of the NO emission in both data sets and in the range of peak brightness and peak altitude. We emphasize that our data set increases the number of positive NO detections by factor of 5, expanding both the latitudinal and seasonal coverage. These new measurements extend above 60° latitude, as well as covering a much broader seasonal range, expanding the existing observations from Cox *et al.* [2008]. There are more detections of NO emission during the first Martian year, MY27, than later during MY28 and MY29, and this interannual variability could be linked to the solar cycle.

[26] The NO intensities from LMD-MGCM are in general agreement with the observations, indicating that the main features of production of NO are captured by the model. We note, however, two important discrepancies between data and model that deserve further investigation. The first discrepancy is the north-south asymmetry present in the data, which does not seem to be in the model. Three departures from symmetry may be visualized by the scatter of the observations from the sine curve $-80 \cdot \sin(L_s)$. First, the “NO polar season” seems to be much shorter for the Southern Hemisphere than for the Northern Hemisphere. This is surprising since the southern winter is longer than the northern winter, due to orbit eccentricity. In the south, there are more than 50 detections poleward of -60° , while there are less than 10

poleward of 60° in the north. Second, as noted above, the lowest altitude is increasing from the South Pole to the North Pole. We know that there is a major difference between the halves of the Martian year, the second half being the season of large dust storms. One might speculate that in the second part of the year, convection, which lifts dust to altitudes up to several tens of kilometers, is somewhat perturbing the descent of air from higher altitudes, triggering by compensation some descent of air at low latitudes where it is not predicted by the model.

[27] The second, and perhaps more important, discrepancy is the absence of simultaneous detections at both poles of a strong NO emission. Both model maps of NO (Figure 5) and O₂ (from Bertaux *et al.* [2012]) indicate that at the equinoxes, there are two simultaneous descents of air in both poles, revealing the existence of two Hadley cells in the thermosphere, extending from the equator to both poles. At other seasons, there is only one cell ascending from the summer hemisphere and descending in the polar regions where CO₂ is condensing on the ground. The strongest emissions in both the modeled NO and O₂ are at the equinoxes. While there are indeed observations of the O₂ emission at both poles during equinox conditions from CRISM data [Clancy *et al.*, 2012], supporting the scheme of two cells for the O₂ emission, it seems that the same circulation pattern is not supported by the absence of detection of NO emission at the poles during equinox (at least at $L_s=180^\circ$). This is rather surprising since the same circulation produces both O₂ and NO emissions. We note, however, two basic differences which might help to understand the discrepancy. N₂ requires more energetic photons (80–100 nm) than CO₂ for photodissociation, and these photons are shielded by CO₂ absorption. Consequently, the altitude range of production of N atoms is above the bulk CO₂ atmosphere, at 130–140 km, as demonstrated by results from the photochemical model that includes nitrogen and ionospheric chemistry (not shown here). This is well above the altitude range of production of O atoms, with peaks at 70–90 km. Therefore, the discrepancies between the model and the observations suggest that it is the high-altitude part of the global circulation model, relevant to the altitude range of N production, which would have to be adjusted. Another difference is that the O₂ recombination requires the presence of a CO₂ molecule to stabilize the reaction, but NO recombination does not. As discussed in Bertaux *et al.* [2012], an air parcel with a certain mixing ratio ρ , when descending, will produce an O₂ emission proportional to $\rho(O)^3$, while for NO, the emission will depend on the product of $\rho(O) \times \rho(N)$ and therefore will be less sensitive to descent of air. A more detailed investigation of these data-model discrepancies is beyond the scope of this paper but remains a potential topic for future work.

[28] **Acknowledgements.** M.-È. Gagné is grateful to the Fonds Québécois de la Recherche sur la Nature et les Technologies (FQRNT) for funding this research. She would also like to thank Dr. Emilie Royer for her help with the preliminary data processing. F Gonzalez-Galindo is funded by a CSIC JAE-Doc contract co-financed by the European Social Fund and by the Spanish MICINN project AYA2012-39691-C02-01.

References

- Bell, J. M., S. W. Bougher, and J. R. Murphy (2007), Vertical dust mixing and the interannual variations in the Mars thermosphere, *J. Geophys. Res.*, 112, E12002, doi:10.1029/2006JE002856.
- Bertaux, J.-L., et al. (2005), Nightglow in the upper atmosphere of Mars and implications for atmospheric transport, *Science*, 307(5709), 566–569.

- Bertaux, J.-L., et al. (2006), SPICAM on Mars Express: Observing modes and overview of UV spectrometer data and scientific results, *J. Geophys. Res.*, *111*, E10S90, doi:10.1029/2006JE002690.
- Bertaux, J.-L., B. Gondet, F. Lefèvre, J.-P. Bibring, and F. Montmessin (2012), First detection of O₂ 1.27 μm nightglow emission at Mars with OMEGA/MEX and comparison with general circulation model predictions, *J. Geophys. Res.*, *117*, E00J04, doi:10.1029/2011JE003890.
- Bertaux, J.-L., M.-E. Gagné, F. Montmessin, F. González-Galindo, and F. Lefèvre (2013), New nitric oxide (NO) nightglow measurements with SPICAM/MEX as a tracer of Mars upper atmosphere circulation, EGU Gen. Assem., Vol. 15, EGU2013-9162.
- Clancy, R. T., et al. (2012), Extensive MRO CRISM observations of 1.27 μm O₂ airglow in Mars polar night and their comparison to MRO MCS temperature profiles and LMD GCM simulations, *J. Geophys. Res.*, *117*, E00J10, doi:10.1029/2011JE004018.
- Connes, P., J. F. Noxon, W. A. Traub, and N. P. Carleton (1979), O₂(¹Δ) emission in the day and night airglow of Venus, *Astrophys. J.*, *233*(1), L29–L32.
- Cox, C., A. Saglam, J.-C. Gérard, J.-L. Bertaux, F. González-Galindo, F. Leblanc, and A. Reberac (2008), Distribution of the ultraviolet nitric oxide Martian night airglow: Observations from Mars Express and comparisons with a one-dimensional model, *J. Geophys. Res.*, *113*, E08012, doi:10.1029/2007JE003037.
- Du, M. L., and A. Dalgarno (1990), The radiative association of N and O atoms, *J. Geophys. Res.*, *95*(A8), 12,265–12,268, doi:10.1029/JA095iA08p12265.
- Feldman, P. D., H. W. Moos, and J. T. Clarke (1979), Identification of the UV nightglow from Venus, *Nature*, *279*(5710), 221–222.
- Gagné, M.-E. (2013), Understanding oxygen photochemistry in CO₂-dominated atmospheres, PhD thesis, Department of Physics, University of Toronto, <http://hdl.handle.net/1807/35824>.
- González-Galindo, F., F. Forget, M. A. López-Valverde, M. Angelats i Coll, and E. Millour (2009), A ground-to-exosphere Martian general circulation model: 1. Seasonal, diurnal, and solar cycle variation of thermospheric temperatures, *J. Geophys. Res.*, *114*, E04001, doi:10.1029/2008JE003246.
- González-Galindo, F., A. Määttänen, F. Forget, and A. Spiga (2011), The Martian mesosphere as revealed by CO₂ cloud observations and General Circulation Modeling, *Icarus*, *216*(1), 10–22, doi:10.1016/j.icarus.2011.08.006.
- Lefèvre, F., S. Lebonnois, F. Montmessin, and F. Forget (2004), Three-dimensional modeling of ozone on Mars, *J. Geophys. Res.*, *109*, E07004, doi:10.1029/2004JE002268.
- Lopez-Valverde, M. A., G. Sonnabend, M. Sornig, and P. Kroetz (2011), Modelling the atmospheric CO₂ 10-μm non-thermal emission in Mars and Venus at high spectral resolution, *Planet. Space Sci.*, *59*(10, SI), 999–1009, doi:10.1016/j.pss.2010.11.011.
- Quémerais, E., J.-L. Bertaux, O. Korablev, E. Dimarellis, C. Cot, B. R. Sandel, and D. Fussen (2006), Stellar occultations observed by SPICAM on Mars Express, *J. Geophys. Res.*, *111*, E09S04, doi:10.1029/2005JE002604.
- Royer, E., F. Montmessin, and J.-L. Bertaux (2010), NO emissions as observed by SPICAV during stellar occultations, *Planet. Space Sci.*, *58*(10), 1314–1326.
- Spiga, A., F. González-Galindo, M. A. López-Valverde, and F. Forget (2012), Gravity waves, cold pockets and CO₂ clouds in the Martian mesosphere, *Geophys. Res. Lett.*, *39*, L02201, doi:10.1029/2011GL050343.
- Stewart, A. I., D. E. Anderson, L. W. Esposito, and C. A. Barth (1979), Ultraviolet spectroscopy of Venus: Initial results from the Pioneer Venus Orbiter, *Science*, *203*(4382), 777–779.
- Sun, Y., and A. Dalgarno (1996), Infrared emission spectra of nitric oxide following the radiative association of nitrogen atoms and oxygen atoms, *J. Quant. Spectrosc. Radiat. Transfer*, *55*(2), 245–249.